

# THE FREQUENCY OF FIELD BLUE-STRAGGLER STARS IN THE THICK DISK AND HALO SYSTEM OF THE GALAXY

RAFAEL M. SANTUCCI

Departamento de Astronomia - Instituto de Astronomia, Geofísica e Ciências Atmosféricas, Universidade de São Paulo, São Paulo, SP 05508-900, Brazil

VINICIUS M. PLACCO

Gemini Observatory, Hilo, HI 96720, USA

SILVIA ROSSI

Departamento de Astronomia - Instituto de Astronomia, Geofísica e Ciências Atmosféricas, Universidade de São Paulo, São Paulo, SP 05508-900, Brazil

TIMOTHY C. BEERS

Department of Physics and JINA Center for the Evolution of the Elements, University of Notre Dame, 225 Nieuwland Science Hall, Notre Dame, IN 46556, USA

HENRIQUE M. REGGIANI

Departamento de Astronomia - Instituto de Astronomia, Geofísica e Ciências Atmosféricas, Universidade de São Paulo, São Paulo, SP 05508-900, Brazil

YOUNG SUN LEE

Department of Astronomy and Space Science, Chungnam National University, Daejeon 305-764, Republic of Korea

XIANG-XIANG XUE

Max-Planck-Institute for Astronomy Königstuhl 17, D-69117, Heidelberg, Germany, and  
Key Lab of Optical Astronomy, National Astronomical Observatories, CAS, 20A Datun Road, Chaoyang District, 100012, Beijing, China

DANIELA CAROLLO

INAF - Osservatorio Astrofisico di Torino, Via Osservatorio 20, Pino Torinese, 10020 Torino, Italy  
*Draft version July 18, 2018*

## ABSTRACT

We present an analysis of a new, large sample of field blue-straggler stars (BSSs) in the thick disk and halo system of the Galaxy, based on stellar spectra obtained during the Sloan Digital Sky Survey (SDSS) and the Sloan Extension for Galactic Understanding and Exploration (SEGUE). Using estimates of stellar atmospheric parameters obtained from application of the SEGUE Stellar Parameter Pipeline, we obtain a sample of some 8000 BSSs, which are considered along with a previously selected sample of some 4800 blue horizontal-branch (BHB) stars. We derive the ratio of BSSs to BHB stars,  $F_{\text{BSS/BHB}}$ , as a function of Galactocentric distance and distance from the Galactic plane. The maximum value found for  $F_{\text{BSS/BHB}}$  is  $\sim 4.0$  in the thick disk (at  $3 \text{ kpc} < |Z| < 4 \text{ kpc}$ ), declining to on the order of  $\sim 1.5 - 2.0$  in the inner-halo region; this ratio continues to decline to  $\sim 1.0$  in the outer-halo region. We associate a minority of field BSSs with a likely extragalactic origin; at least 5% of the BSS sample exhibit radial velocities, positions, and distances commensurate with membership in the Sagittarius Stream.

*Subject headings:* Galaxy: halo—methods: spectroscopy—methods: radial velocities—stars: blue stragglers—stars: blue horizontal branch—stars: binaries

## 1. INTRODUCTION

Blue-straggler stars (BSSs) lie brighter and blueward of the main-sequence turnoff region in color-magnitude diagrams of globular and open clusters. This is a region where, if the BSSs are single stars, they should have already evolved away from the main sequence. Since they lie blueward of the cluster turnoff point, and ap-

pear to linger (or straggle behind already evolved stars), they have been traditionally referred to as blue stragglers (Sandage 1953). BSSs have been found in all stellar populations and environments, including: Population I stars in the field (Carney et al. 2005), in open clusters of all ages (de Marchi et al. 2006), and among thick-disk stars (Fuhrmann & Bernkopf 1999), as well as among Population II stars in globular clusters (Piotto et al. 2004), the

Galactic halo (Preston et al. 1994), the Galactic bulge (Clarkson et al. 2011), and dwarf galaxies in the Local Group (Momany et al. 2007).

Since their discovery, a large number of studies and reviews have been published discussing the detection of BSSs, their properties, and various hypotheses to account for the blue-straggler phenomenon (Leonard 1989; Stryker 1993; Baily 1995; Leonard 1996; Preston 2014). Two mechanisms for their origin have been most prominently mentioned: (i) Collisions between stars, resulting in a more massive and apparently younger star (Hills & Day 1976); and (ii) coalescence and/or mass-transfer processes in binary systems, initially proposed by McCrea (1964). The latter scenario appears to be the main channel for the formation of BSSs, where the more-massive star in a binary system transfers material, during its post main-sequence stage, to its presently-observed companion (Boffin et al. 2014). The companion star, now more massive, appears anomalously younger.

Fusi Pecci et al. (1992) were among the first to propose that BSSs in different environments may have different origins. In globular clusters, both of the aforementioned processes could act simultaneously. Collisions are expected to dominate in the central regions, while in the outer regions, BSSs mass transfer dominates. As shown by Mapelli et al. (2004), the specific frequency of BSSs in globular clusters appears highly peaked at cluster centers, and rapidly decreases at intermediate radii; it rises again in the outer regions of most globular clusters.

A contrasting trend is found when comparing the frequency of BSSs in different environments (Preston et al. 1994; Momany et al. 2007); denser stellar environments (globular clusters) exhibit BSS frequencies that are lower than in less-dense stellar environments (open clusters and the Galactic field). One explanation for this observation suggests that multiple systems (presumably the progenitors of BSSs) can be more easily disrupted when subjected to gravitational interactions within the clusters (Preston & Sneden 2000). Even the stars found in the low-density outer regions of globular clusters may be subject to stellar encounters if their intra-cluster motions carry them into the central high-density regions.

Preston & Sneden (2000) argued that field BSSs were created primarily by mass-transfer processes. They noted that field BSSs are much more common per unit luminosity than BSSs in the lower-density outer regions of globular clusters. Binary systems, even in those low-density regions, may have already been destroyed, which would reduce the number of BSSs. Preston & Sneden (2000) obtained high-resolution spectroscopy for 62 of the 84 so-called blue metal-poor (BMP) stars brighter than  $B \sim 15$  from Preston et al. (1994). These stars exhibit main-sequence gravities and colors bluer than most metal-poor globular cluster turnoffs,  $0.15 < (B - V)_0 < 0.35$ . Preston & Sneden (2000) concluded that over 60% of their sample are binaries, and that at least 50% of them are BSSs. These values suggest that the BSSs can be a strong indicator of the presence of binary systems, and can be used as probe of the binarity (in particular close binaries) of the stellar populations in the Galaxy.

Gaspey et al. (1994) obtained moderate-resolution spectra of the Li 6707 Å doublet for a sample of likely

field BSSs, and obtained clear evidence for Li depletion, concluding that this depletion is a general property associated with blue stragglers. These authors argued that the origin of the Li depletion in their sample stars was likely related to large-scale mixing, presumably associated with the formation of blue stragglers.

Ryan et al. (2001) and Ryan et al. (2002) have also argued in favor of the binarity of field blue stragglers, based on consideration of the so-called ultra-Li-deficient halo stars, proposing that these stars may have had their surface abundances of lithium reduced by the same mechanism that produces field blue stragglers. These ultra-Li-deficient halo stars were shown to possess more rapid rotation than other ancient metal-poor stars, with the spin-up likely due to the mass-transfer process, and/or chemical peculiarities associated with mass transfer from an AGB progenitor. The Ryan et al. sample of stars were cooler than the main-sequence turnoff, hence they were referred to by these authors as “blue stragglers to be.” These stars thus could be viewed as the low-mass counterpart of field blue stragglers (Ryan et al. 2002). Furthermore, the process of mass transfer that appears to be responsible for creating BSSs must act in cooler stars as well. Rocha-Pinto et al. (2001) identify cooler blue-straggler candidates (yellow or red stragglers). These were referred to as *chromospherically young and kinematically old stars* (CYKOS).

It is worth noting that the BSS frequency in low-luminosity dwarf galaxies and open clusters ( $N_{\text{BSS}}/N_{\text{BHB}} \sim 2.2$ ; Momany et al. 2007) is different than that derived for the Galactic halo ( $N_{\text{BSS}}/N_{\text{BHB}} \sim 4$ ; Preston et al. 1994). However, as pointed out by Momany et al. (2007), the latter value was found based on a sample of only 62 BMP stars distributed along different lines of sight, located at different distances, and for which no observational star-by-star (BSS/BHB) correspondence could be defined.

Furthermore, field-star samples have introduced another puzzle, one at least as intriguing as the blue straggler phenomenon itself. Preston et al. (1994), Preston & Sneden (2000) and Carney et al. (2001, 2005) argued that binary-star evolution and mass transfer is one path for the creation of blue stragglers, and apparently the most common among field stars. However, some metal-poor main-sequence field stars that are hotter than globular-cluster main-sequence turnoffs are apparently *not binaries* (see Preston et al. 1994, for further details). These authors accounted for their existence as the debris from accreted dwarf satellite galaxies whose star formation continued over an extended period.

This paper aims to examine the issues previously raised concerning field BSSs by gathering a large new sample of BSS candidates, in order to improve estimates of the specific frequency of  $N_{\text{BSS}}/N_{\text{BHB}}$  ( $F_{\text{BSS/BHB}}$ ) in the Galactic field, and to test the hypothesis of the extragalactic origin for some BSSs. This paper is outlined as follows. Section 2 describes the assembly of the database used to identify our sample of field BSSs and BHB stars, and the photometric restrictions adopted for both samples. Section 3 summarizes our analysis of the selected spectra, and the techniques used to partition them into these two

<sup>1</sup>  $N_{\text{BSS}}$  and  $N_{\text{BHB}}$  are the number of BSSs and BHB stars found in these environments, respectively.

groups. Section 4 derives estimates for the absolute magnitudes and distances for both BSSs and BHB stars, and evaluates their frequencies in the Galactic field. Section 5 presents a kinematic analysis of the field BSS sample, in an attempt to associate their radial velocities with stellar streams. A brief discussion and our conclusions are provided in Section 6.

## 2. PHOTOMETRIC SELECTION AND STELLAR PARAMETERS

### 2.1. SDSS – DR8

The Sloan Digital Sky Survey (SDSS; York et al. 2000) is a large photometric and spectroscopic survey that covers about one-quarter of the northern sky. This paper makes use of the eighth data release (DR8), which contains the data obtained by the survey through January 2011 (Aihara et al. 2011). The first restrictions adopted in the selection of field BSSs and BHB stars follow the same criteria used by Xue et al. (2008).

### 2.2. Color Cuts

Blue-straggler and blue horizontal-branch candidates are often identified in the SDSS color-color diagram region with the following color cuts:  $0.60 < (u - g) < 1.60$  and  $-0.50 < (g - r) < 0.05$  (Xue et al. 2008; Deason et al. 2011). This region is preferentially populated by A-type stars. For this work, we first obtained a sample of 19771 objects within these color limits, and with available spectra, but with no restrictions on apparent magnitudes or location on the sky within the SDSS footprint, and covering the range  $14.5 < g < 21$ , the bright limit being set by saturation in the SDSS imaging scans. Note that the *ugriz* magnitudes and color indices are all corrected for absorption and reddening using the extinction maps from Schlegel et al. (1998).

Previous efforts to study stars in this color region usually targeted only BHB stars (Sirko et al. 2004; Xue et al. 2008; Deason et al. 2011; Xue et al. 2011). In this work, we are interested in selecting both BSS and BHB candidates. However, photometry alone does not uniquely distinguish main-sequence A-type stars (of which the metal-poor stars are BSS candidates) from giant (BHB) candidates. Furthermore, in this color region, the A-type stars can be mixed with stars of cooler spectral types, such as metal-poor F- and G-type stars. Thus, we also made use of available spectroscopy to trim our sample, as described below.

### 2.3. Stellar Parameters

The spectra of the selected sample have stellar parameters determined by the current version of the SEGUE Stellar Parameter Pipeline (SSPP, Lee et al. 2008a,b; Allende Prieto et al. 2008; Smolinski et al. 2011; Lee et al. 2011). From the SSPP, we obtained values of effective temperature ( $T_{\text{eff}}$ ), surface gravity ( $\log g$ ), metallicity ( $[\text{Fe}/\text{H}]^2$ ), and heliocentric radial velocity ( $V_{\text{HRV}}$ ). To select the best BSS candidates (as opposed to foreground A-type stars in the disk populations), we applied

<sup>2</sup> The abundance of an element in relation to another is defined in the usual manner, using the notation:  $[A/B] = \log(N_A/N_B)_* - \log(N_A/N_B)_\odot$ , where  $N_A$  and  $N_B$  are the number of atoms of elements A and B in the star ( $*$ ) and in the Sun ( $\odot$ ), respectively.

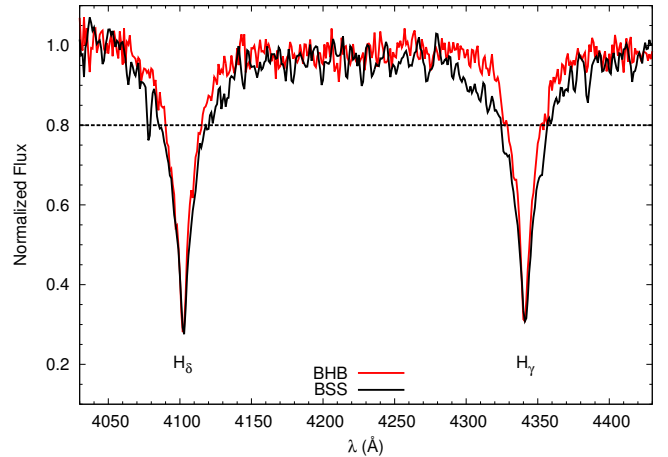


FIG. 1.— Normalized spectrum of a BHB star (red line) and a BSS (black line) for the same  $T_{\text{eff}}$  ( $\sim 8100$  K) in the  $H_\gamma$ - $H_\delta$  region. The dashed line is drawn at 20% below the continuum, highlighting the difference between the Balmer-line wings.

a restriction in metallicity,  $[\text{Fe}/\text{H}] < -0.4$ , reducing the sample to 18560 objects.

It is relatively straightforward to identify BSSs in globular clusters because the horizontal-branch stars, whose colors blend with hotter main-sequence stars, are seen at different apparent magnitudes (BHB stars are typically  $\sim 2$  magnitudes brighter than BSSs, as noted by Preston et al. 1994; Deason et al. 2012). Unfortunately, these two populations cannot be easily separated in the field, because the stars are not at the same distance.

In the temperature range of A-type stars, the Balmer lines are the main tool to separate A-type main-sequence from giant stars (BSSs from BHB stars, respectively). The temperature modifies the depth of the Balmer lines, while the surface gravity changes the width of its wings (as initially noted by Pier 1983). These effects have a clear impact on the appearance of the spectrum, as shown in Figure 1: for stars with the same  $T_{\text{eff}}$  (in this case,  $\sim 8100$  K), the Balmer-line wings are broader for higher surface gravities.

## 3. THE BLUE-STRAGGLER AND BLUE HORIZONTAL-BRANCH SAMPLES

In this section we describe the methods used to separate BSSs from BHB stars, using the available medium-resolution SDSS/SEGUE spectroscopy. Deason et al. (2012) states that the differences between BSSs and BHB stars becomes most evident for spectra with  $S/N > 5$  (see the bottom panels in Figure 3 of Deason et al. 2012). For this work, we prefer to only use stars with spectra having an average signal-noise ratio (over the optical spectrum) of  $(S/N) \geq 10$ . This limit allows for a confident distinction between BSSs and BHB stars where they are photometrically indistinguishable, and for the reliable stellar parameters from the SSPP.

Using the parameters calculated by the SSPP, we can compare the surface gravities and effective temperatures of BSSs with BHB stars (similar to Wilhelm et al. 1999; Deason et al. 2012). However, the atmospheric parameters calculated for stars with temperatures above 7500 K (where the BSSs and BHB stars are usually found) require additional quantitative validation. This is accom-

plished by comparing the results of the SSPP with other methods for separating the BSSs from BHB stars, which generally required higher S/N spectra, typically greater than  $\sim 15$  (values typically achieved for SDSS spectra of stars with apparent magnitudes  $g < 18$ ).

It is also important to note that, even though stars with  $g > 18$  are usually not suitable for analysis by all the methods presented below, they provide valuable information on the populations of BSSs and BHB stars (especially since, as shown below, the majority of likely BSSs in our sample are fainter than  $g = 17$ ). For the following analysis, we divided the sample in two: (i) The Bright Sample ( $g < 18$ ) and (ii) the Faint Sample ( $g \geq 18$ ).

### 3.1. The Bright Sample: $14.5 < g < 18$

Since the Bright Sample contains stars having spectra with higher S/N ratios, it is possible to apply a series of quantitative tests to distinguish between BSSs and BHB stars. These are described below.

#### 3.1.1. SSPP Restrictions

The parameters provided by the SSPP were used to identify BSSs and BHB stars. Since the Balmer lines are strong in the  $7500 \text{ K} < T_{\text{eff}} < 10000 \text{ K}$  range, it is possible to effectively distinguish between BSSs and BHB stars from their  $\log g$  distribution (Wilhelm et al. 1999). Figure 2 summarizes the adopted restrictions. The line separating these two groups of A-type stars is  $\log g = 3.80$ , as estimated from the  $\log g$  distributions, for stars with  $g < 18$  (see top panel of Figure 5). This value represents a threshold at which, statistically, the contamination of the BSS population by BHB stars is minimal. The limits lie at  $3\sigma$  from the peaks in the top panel of Figure 5 centered at  $\log g = 3.38$  ( $\sigma = 0.14$  dex) and  $\log g = 4.33$  ( $\sigma = 0.18$  dex), which represent the BHB stars and BSSs, respectively.

#### 3.1.2. The $f_m$ vs. $D_{0.2}$ Method

The parameters used in the following analysis are obtained through fits to a Sersic profile (Sersic 1968), which describes the shape of the Balmer spectral features (Clewley et al. 2002):

$$S(x) = n - a \cdot \exp[-(|\lambda - \lambda_0|/b)^c], \quad (1)$$

where,  $n$ ,  $a$ ,  $b$ , and  $c$  are free parameters. The parameter  $n$  fits the continuum level ( $\sim 1$  for our normalized spectra),  $\lambda_0$  is the wavelength at the line center, and  $a$  defines the scale-depth parameter. The parameters  $b$  (scale width) and  $c$  (scale shape) will be subsequently examined. They are used in the scale width-shape method (Clewley et al. 2002), as described in Section 3.1.3.

There is no fundamental relation between  $a$  and the other Sersic parameters, but the  $a$  values have well-defined Gaussian distributions around a mean value for each Balmer line. For our sample, these average values are:  $\langle a_\beta \rangle = 0.709$ ,  $\langle a_\gamma \rangle = 0.694$ , and  $\langle a_\delta \rangle = 0.769$ . We refined the estimated Sersic profile parameters by re-adjusting the function with  $\langle a \rangle$  fixed for each line.

The  $f_m$  versus  $D_{0.2}$  method was first proposed by Pier (1983); it compares  $T_{\text{eff}}$  and  $\log g$  indirectly, by measuring specific quantities in the stellar spectra. The parameter  $f_m$  is the deepest flux relative to the continuum level,

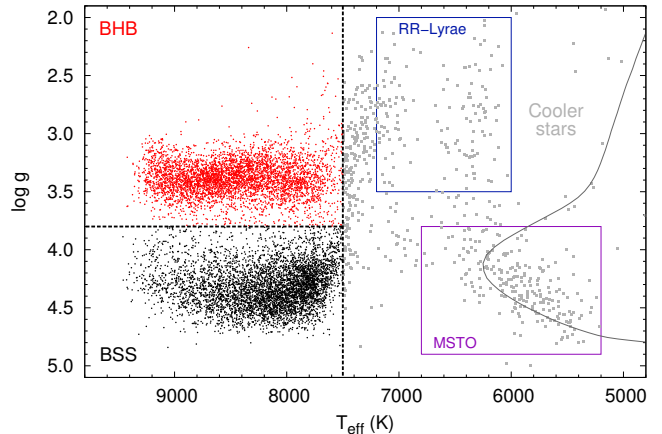


FIG. 2.— Distribution of the SSPP  $T_{\text{eff}}$  vs.  $\log g$  for stars with  $g < 18$ . There are two stellar groups concentrated in  $T_{\text{eff}} \geq 7500 \text{ K}$ : one for  $\log g \sim 3.4$  (BHB stars: red dots) and other with  $\log g \sim 4.3$  (BSSs: black dots). The gray squares are cooler stars and are not considered further in our analysis. For convenience of the reader, we highlight the positions where the RR Lyrae stars are often found using the blue rectangle (Wilhelm et al. 1999), where the gap with no stars present is the expected location of the instability strip; the purple rectangle shows the region where the occupied by main-sequence turnoff stars (MSTO). Overplotted is a Yale-Yonsei isochrone (Demarque et al. 2004) for 12 Gyr and  $[\text{Fe}/\text{H}] = -2.0$ .

usually measured at the center of the line (it is sensitive to  $T_{\text{eff}}$ ). The parameter  $D_{0.2}$  is the width of the line measured at 20% below the adjusted continuum level (Beers et al. 1992; Sirko et al. 2004), and provides an indicator of  $\log g$ . As seen in Figure 1, when  $\log g$  is higher, the greater  $D_{0.2}$  becomes. To obtain  $D_{0.2}$ , we subtracted the roots of the inverse function when  $S(x) = 0.8n$ , following Clewley et al. (2002), which yields:

$$D_{0.2} = 2 \cdot b \cdot [\log(n/(5 \cdot \langle a \rangle))]^{\frac{1}{c}}. \quad (2)$$

We adopted the  $H_\delta$  feature to compare the parameters  $f_m$  and  $D_{0.2}$  for this method, indicated by  $\delta$  in the subscript of the derived parameters (see Sirko et al. 2004, for further details). Figure 3 shows the behavior of  $D_{0.2\delta}$ , as a function of  $f_{m\delta}$ , for stars with  $g < 18$ . The stars concentrated at  $(f_{m\delta}; D_{0.2\delta}) \sim (0.26; 25)$  are the BHB stars; the stars with larger  $D_{0.2\delta}$  are BSSs. The remaining stars have cooler spectral types.

To compare the restrictions adopted by the SSPP with the limits in the  $f_m$  vs.  $D_{0.2}$  method, we identified the stars in Figure 3 according to the regions described in Figure 2; black dots represent BSSs, red dots are BHB stars, and the gray squares are cooler stars. Note that these divisions exhibit good agreement with the separation based on the SSPP stellar-parameter values ( $\sim 92\%$  of stars satisfy both restrictions).

#### 3.1.3. The Scale Width-Shape Method: $c$ vs. $b$

An additional method often adopted to separate BSSs from BHB stars is the scale width-shape method ( $c$  vs.  $b$ ), first described by Clewley et al. (2002). This method separates these stars through the parameters set by the Sersic profile (with the parameter  $a$  fixed). In order to apply this approach, we calculated the average of the parameters  $c$  and  $b$  for the  $H_\beta$ ,  $H_\gamma$  and  $H_\delta$  lines, fol-



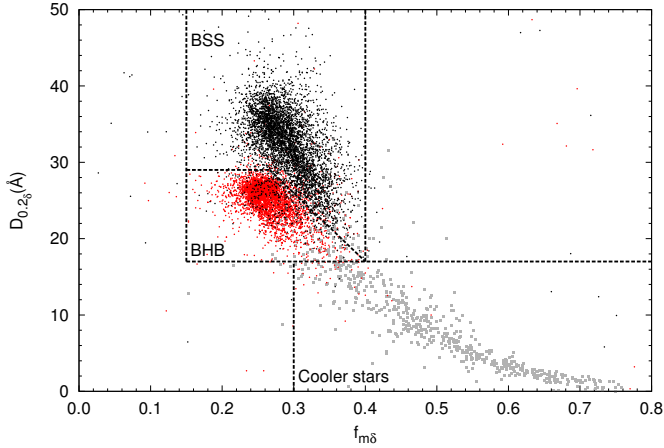


FIG. 3.— Comparison of  $f_{m\delta}$  vs.  $D_{0.2\delta}$ , color-coded according to the restrictions adopted by the SSPP (Figure 2). The distributions of BSSs and BHB stars exhibit some overlap beyond the adopted limits (dashed lines). The adopted criteria to select BSSs are: (i)  $0.15 < f_{m\delta} < 0.27$ ,  $D_{0.2\delta} > 29$ ; (ii)  $0.27 < f_{m\delta} < 0.40$ ,  $D_{0.2\delta} > -90 \cdot f_{m\delta} + 53$ . Accordingly, the criteria for BHB candidates are: (i)  $0.15 < f_{m\delta} < 0.27$  and  $17 < D_{0.2\delta} < 29$ ; (ii)  $0.27 < f_{m\delta} < 0.40$  and  $17 < D_{0.2\delta} < -90 \cdot f_{m\delta} + 53$ .

lowing Deason et al. (2011). The average of these parameters is shown in Figure 4, where  $c_{\beta\gamma\delta}$  and  $b_{\beta\gamma\delta}$  are color-coded by the adopted regions described in Figure 2. As can be seen, there is good agreement when comparing this method with separation based on the SSPP stellar-parameter values ( $\sim 95\%$  of stars satisfy both restrictions). We note that the parameters  $b$  and  $c$  could be used, in principle, by themselves to separate BSS from BHB (see Preston 2014). The mixed stars that passed the initial color cuts now exhibit a clear separation in the  $c_{\beta\gamma\delta}$  versus  $b_{\beta\gamma\delta}$  plane; the gap between them distinguishes between BSSs and BHB stars, as defined by a fourth-order polynomial:

$$b_{\beta\gamma\delta} = +9.20 - 46.32 \cdot (c_{\beta\gamma\delta}) + 82.24 \cdot (c_{\beta\gamma\delta})^2 - 23.36 \cdot (c_{\beta\gamma\delta})^3 - 10.82 \cdot (c_{\beta\gamma\delta})^4. \quad (3)$$

To select BSSs with  $g < 18$ , we combined the SSPP restrictions,  $f_m$  vs.  $D_{0.2}$ , and the scale width-shape method. Whereas the constraints of the SSPP proved fully compatible with the methods based on the analysis of the Balmer lines, we further restrict the BSS and BHB candidates according to the limits: BSSs have  $\log g > 3.8$  and the BHB stars lie between  $3.0 \leq \log g \leq 3.8$ . The mean error on effective temperature given by the SSPP is about 150 K (Lee et al. 2008b), which is slightly higher than the average error of the parameters for our sample ( $\sim 130$  K). We selected only the stars with  $T_{\text{eff}} \geq 7650$  K. The stars satisfying these cuts are within  $3\sigma$  of the mean of both peaks in  $\log g$ , as shown in the top panel of Figure 5, resulting in 4838 BSSs and 4380 BHB stars.

### 3.2. The Faint Sample: $18 < g < 21$

The traditional methods ( $f_m$  vs.  $D_{0.2}$ , and  $c$  vs.  $b$ ) cannot properly evaluate the stars in our sample with  $g > 18$ , due to the lower  $\langle S/N \rangle$  ratios in SDSS/SEGUE spectra of these fainter stars (Clewley et al. 2002; Sirko et al. 2004). Thus, for the 5663 stars in the Faint Sample,

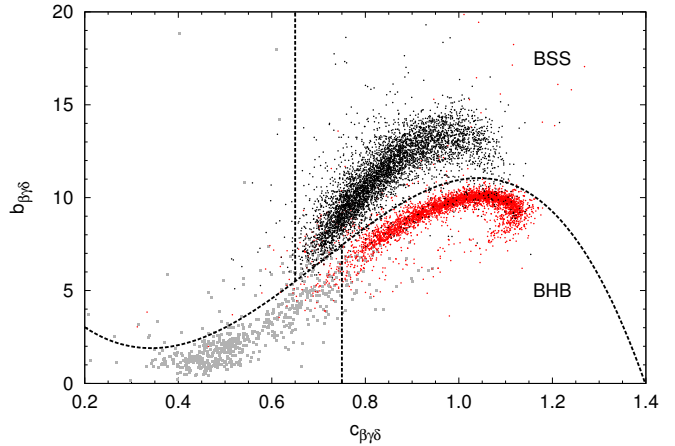


FIG. 4.— Comparison between  $c_{\beta\gamma\delta}$  and  $b_{\beta\gamma\delta}$ , with color-coding according to the restrictions adopted by the SSPP. As verified with the  $f_m$  vs.  $D_{0.2}$  method, the limits adopted by the SSPP for separating the BSSs and BHB stars agree very well ( $\sim 95\%$  of stars satisfy both restrictions). The limit line that separates these two groups is defined by the fourth-order polynomial given by Equation 3.

we employed only the SSPP parameters to separate the BSSs and BHB stars.

The  $\log g$  distribution for the Faint Sample is shown in the lower panel of Figure 5. The peak centered at  $\log g = 3.57$ , which represents BHB stars, has a high dispersion ( $\sigma = 0.33$  dex). This increases the size of the overlap region between the two distributions and, if we were to consider the  $3\sigma$  region as a limit, it would exclude almost all BSSs, which are peaked at  $\log g = 4.27$  ( $\sigma = 0.20$  dex).

As the stars analyzed in the lower panel of Figure 5 are also well-described by Gaussian distributions, we assessed the probability of finding BHBs using the peak positions and values up to  $3\sigma$  away from them. The adopted restriction for the BHB distribution is  $\log g < 3.66$  ( $3\sigma$  away from the BSSs peak).

Since our goal is to select BSSs candidates, we adopt a more relaxed criteria to its distribution, even though it leads to greater contamination from the BHB population. Estimating the amount of stars coming from each distribution, we analyzed the contamination for every sigma. For example, there are 3646 stars with  $\log g > 4.27$  (located at  $\log g_{\text{BHB}} + 2\sigma_{\text{BHB}}$ ), but the probability of finding BHB stars in this range of  $\log g$  is approximately 2%. Thus, stars with  $\log g > 4.27$  have a 98% probability of being BSSs.

We conclude that, for  $g > 18$ , the most reliable BHB candidates are found in the surface-gravity range  $3.00 < \log g < 3.66$  (416 objects). Accordingly, for BSSs we adopted the limit of  $\log g > 3.92$ , which is  $1\sigma$  away from the BHB peak, with an average probability of  $\sim 88\%$ .

Combining the Bright and Faint Samples, we obtained a total of 8001 BSS candidates, with an average probability of  $\sim 95\%$ . We also obtained 4796 BHB candidates, with an average probability of correct selection of  $\sim 98\%$ .

Figure 6 shows the distributions of  $\log g$  from the SSPP for our full sample of BSSs and BHB stars, in intervals of apparent magnitude. As is clear from inspection of this sample, the higher gravity BSSs begin to dominate over the lower gravity BHB stars for  $g > 17$ . Figure 7 shows the distribution of derived  $[\text{Fe}/\text{H}]$  for these same stars,

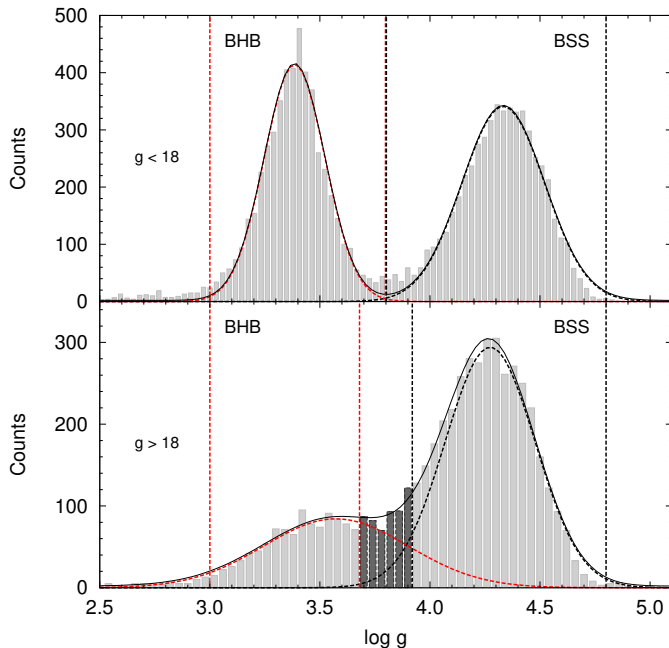


FIG. 5.— Top panel: Distribution of  $\log g$  for stars with  $g < 18$ . The peak centered at  $\log g = 3.38$  ( $\sigma = 0.14$  dex) represents the distribution of BHB stars; that at  $\log g = 4.33$  ( $\sigma = 0.18$  dex) applies to BSSs. Bottom panel: Distribution of  $\log g$  for stars with  $g > 18$ . The peak centered at  $\log g = 3.57$  ( $\sigma = 0.33$  dex) represents the distribution of BHB stars; that at  $\log g = 4.27$  ( $\sigma = 0.20$  dex) represents BSSs. It can be seen that the fraction of BHB stars decays quickly at high surface gravity for the fainter stars.

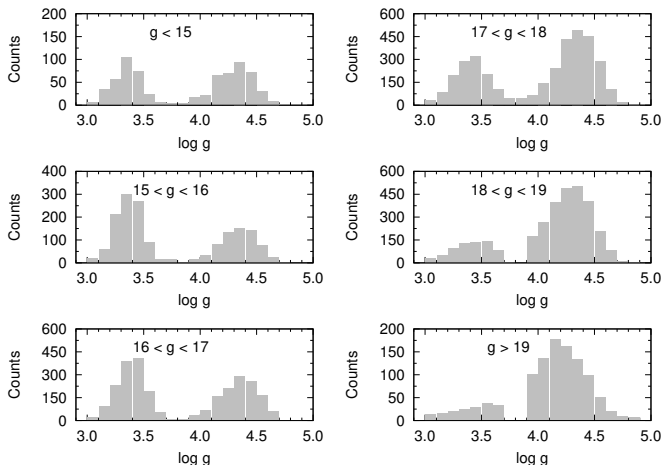


FIG. 6.— Histograms of  $\log g$ , evaluated in different intervals of  $g$ -band apparent magnitude. The number of BSSs dominates over the number of BHB stars at fainter apparent magnitude ( $g > 17$ ).

in this case for the Bright Samples and Faint Samples of BSSs and BHB stars. Although the mean metallicities of the BSSs and BHB stars are similar, the BSSs are more prevalent at higher metallicity than the BHB stars.

#### 4. DISTANCE CALIBRATIONS AND FREQUENCIES

In this section we obtain an absolute magnitude calibration for our full sample of 8001 BSSs and 4796 BHB stars, extending over the magnitude range  $14.5 < g < 21$ .

A number of studies adopt calibrations for apparent magnitudes based on photometric systems other than the

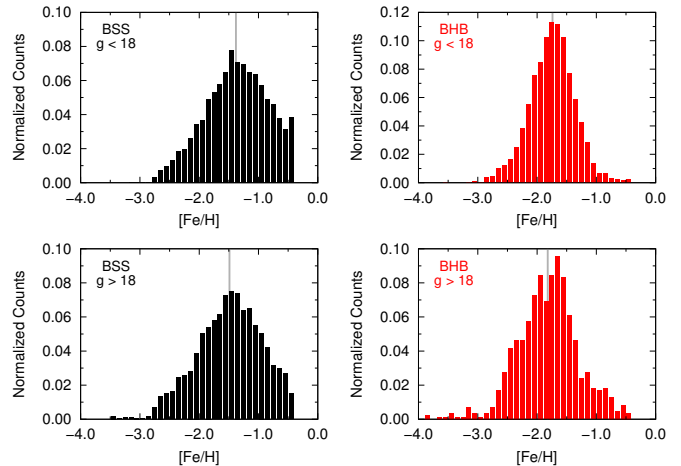


FIG. 7.—  $[\text{Fe}/\text{H}]$  distributions for our sample stars (left panels: BSSs; right panels: BHB stars) for the Bright Sample (upper panels) and the Faint Sample (bottom panels). The gray lines indicate the mean of each  $[\text{Fe}/\text{H}]$  distribution.

SDSS *ugriz* system (e.g., Kinman et al. 1994; Preston et al. 1994; Preston & Snedden 2000; Carney et al. 2001, 2005). In this work, we used the transformations of Zhao & Newberg (2006), which were derived from SDSS stars with known *UBVRI* photometry, including a number of BSSs and BHB stars:

$$V_0 = g - 0.561 \cdot (g - r) - 0.004, \quad (4)$$

and

$$(B - V)_0 = 0.916 \cdot (g - r) + 0.187. \quad (5)$$

According to Beers et al. (2012), the valid range for these conversions is  $-0.5 < g - r < 1.0$ , consistent with the color indices adopted in this work. In addition, the calculated values are within the limits proposed by Carney et al. (2005) to define field BSSs.

#### 4.1. Absolute Magnitudes of Field BSSs

Based on the  $V$ -band magnitude, it is possible to estimate the absolute magnitude for BSSs using the relation from Kinman et al. (1994):

$$M_{V_{\text{BSS}}} = 1.32 + 4.05 \cdot (B - V)_0 - 0.45 \cdot [\text{Fe}/\text{H}]. \quad (6)$$

This relation was first determined from BSSs in globular clusters by the work of Sarajedini (1993, 1994). Assuming  $(B - V)_0 = 0.1$  and  $[\text{Fe}/\text{H}] = -1.7$  as typical values for metal-poor A-type stars selected in this work, we verify that the field BSS candidates have  $M_V \approx 2.5$ . This value is in agreement with blue stragglers observed in globular clusters and dwarf galaxies (Sarajedini 1993; Momany et al. 2007).

Deason et al. (2011) also developed a calibration for the  $g$ -band absolute magnitude for field BSSs. They made use of stars in Stripe 82 that are members of the Sagittarius Stream, combining the apparent magnitudes and the results obtained by Watkins et al. (2009). The latter used RR Lyræ stars to estimate the distance to stars in the stream in the right ascension range  $25^\circ < \alpha < 40^\circ$ , with  $D_{\text{Sgr}} = 26.1 \pm 5.6$  kpc. The absolute-magnitude calibration in the  $g$ -band from Watkins et al. (2009),

$M_{\text{gBSS}} = 3.108 + 5.495 \cdot (g - r)$ , is similar to that presented by Kinman et al. (1994) for  $[\text{Fe}/\text{H}] = -1.5$ , and also agrees with the mean metallicity of stars identified in the Sagittarius Stream ( $[\text{Fe}/\text{H}] = -1.43$ , Watkins et al. 2009). However, unlike the relation used by Kinman et al. (1994), Deason et al. (2011) found no strong dependence on metallicity. This is probably due to the use of BSSs in the Sagittarius Stream, which already have a mean  $[\text{Fe}/\text{H}] = -1.4$ , and also have similar luminosities (Watkins et al. 2009). The adopted error for this calibration is  $\sigma_{M_g} = 0.5$  mag, primarily arising from the expected error in the distance to the Sagittarius Stream.

The distances are systematically smaller for the method calibrated to BSSs in the Sagittarius Stream, but both relations agree within  $2\sigma$ . We adopt the calibration given in Equation 6 of Kinman et al. (1994), because it was determined from BSSs in globular clusters with different metallicities covering a wide range of colors and absolute magnitudes. Furthermore, we take into account that the error in the absolute magnitude of each star is certainly greater for the fainter objects.

#### 4.2. Absolute Magnitudes of Field BHBs

We employed two different calibrations to determine absolute magnitudes for the BHB sample: (1) Deason et al. (2011) derived  $M_g$  using SDSS photometry of 10 globular clusters from An et al. (2008); (2) Fermani & Schönrich (2013) proposed a calibration with a dependence on the metallicity, arguing that the relation adopted by Deason et al. (2011) is systematically fainter for metal-poor stars and brighter for metal-rich stars. The absolute magnitudes for Deason et al. 2011 ( $M_{\text{gD}}$ ) and Fermani & Schönrich 2013 ( $M_{\text{gFS}}$ ) are given by:

$$M_{\text{gD}} = 0.434 - 0.169 \cdot (g - r) + 2.319 \cdot (g - r)^2 + 20.449 \cdot (g - r)^3 + 94.517 \cdot (g - r)^4, \quad (7)$$

$$M_{\text{gFS}} = 0.0075 \cdot e^{-14.0 \cdot (g - r)} + 0.04 \cdot ([\text{Fe}/\text{H}] + 3.5)^2 + 0.25. \quad (8)$$

The range of  $M_g$  for BHB stars in globular clusters evaluated by Deason et al. (2011) is  $0.45 < M_g < 0.65$ , and their metallicities are in the range  $[-2.3 : -1.3]$ . The authors did not find any significant dependence on metallicity for  $M_g$ .

According to Fermani & Schönrich (2013), the lack of metallicity dependence on the absolute magnitude calibration of Deason et al. (2011) is primarily due to uncertainties in their adopted distance moduli, reddening, and presumed systematic differences between clusters and field halo stars; they thus argued that Deason et al. could not rule out a detectable metallicity dependence on field BHB stars. For the distance calculations presented below, we explore both  $M_g$  calibrations.

#### 4.3. The Relative Frequencies of BSSs and BHB Stars

##### 4.3.1. Galactocentric Distances

In order to determine the ratio between BSSs and BHB stars ( $F_{\text{BSS/BHB}}$ ), we first proceed by counting them directly, as a function of their distance from the Galac-

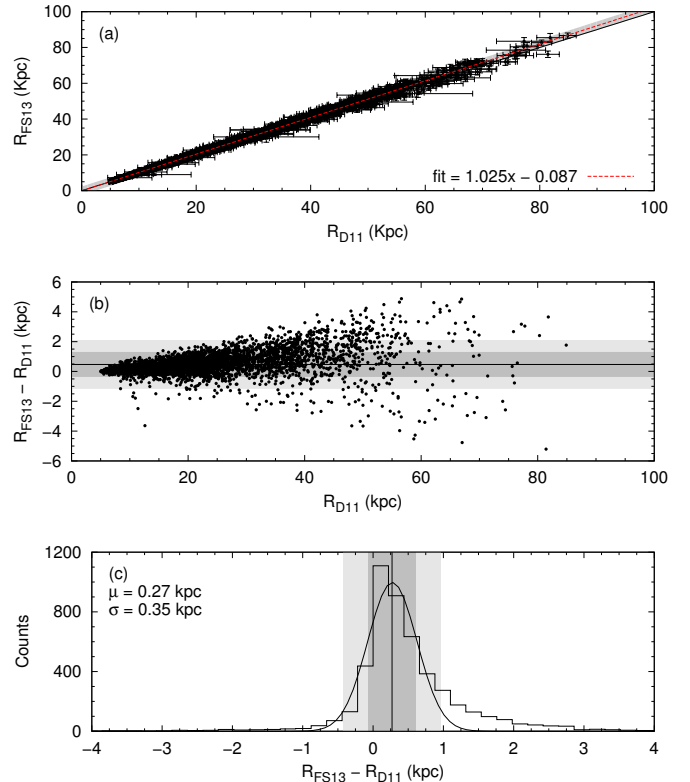


FIG. 8.— (a): Comparison between distances estimated using the absolute magnitude calibrations of Deason et al. (2011) and Fermani & Schönrich (2013). The solid line represents  $R_{\text{FS13}} = R_{\text{D11}}$ , the red dashed line is a linear fit to the data, and the gray region is the  $\pm 3\sigma$  limit of the data. Panels (b) and (c) show, respectively, the residuals for the distribution and its dispersion, represented by a Gaussian fit. The dark gray region represents the limit within  $1\sigma$  of the average value ( $\sim 0.34$  kpc) for the distribution; the light gray region is the limit within  $2\sigma$  of the average value.

tic center. The Galactocentric distance,  $R$ , is calculated based on the distance,  $D$ , from the Sun (in kpc):

$$D = 10^{[(m-M)/5-2]}, \quad (9)$$

and

$$R^2 = (R_\odot - D \cos b \cos l)^2 + (D \sin b)^2 + (D \cos b \sin l)^2, \quad (10)$$

where  $b$  and  $l$  are the Galactic latitude and longitude, respectively, and  $R_\odot$  is the distance of the Sun to the Galactic center. We adopted  $R_\odot = 8.5$  kpc to be consistent with the recent kinematic analysis from Carollo et al. (2010).

Figure 8 compares the Galactocentric distances obtained using the BHB calibrations from Deason et al. (2011) ( $R_{\text{D11}}$ ) and Fermani & Schönrich (2013) ( $R_{\text{FS13}}$ ). The  $R_{\text{FS13}}$  distances are, on average,  $\sim 2.5\%$  larger than  $R_{\text{D11}}$ , which is within the errors for both calibrations. Also, from panels b and c of Figure 8, it is possible to see that, even though there is a larger spread for distances above 40 kpc, there are no trends between the calibrations. The zero-point offset for this comparison is 0.27 kpc, with a standard deviation of 0.39 kpc.

It is clear that the differences between these two ap-

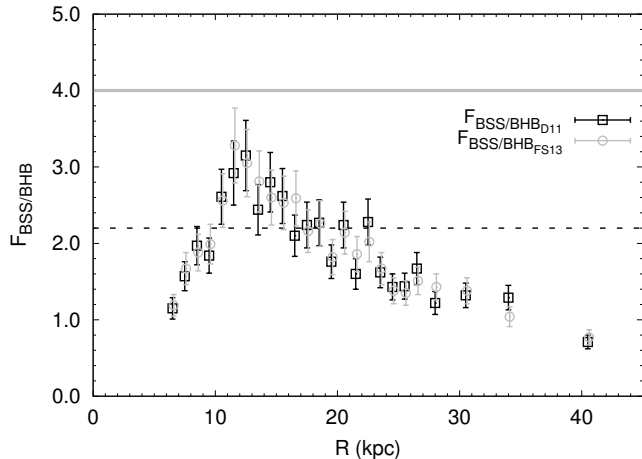


FIG. 9.— Comparison of the “as observed”  $F_{\text{BSS/BHB}}$ , as a function of Galactocentric distance, using the absolute-magnitude calibrations from Deason et al. (2011) and Fermani & Schönrich (2013). The gray line represents the value of  $F_{\text{BSS/BHB}}$  estimated in the Solar Neighbourhood by Preston et al. (1994), and the dashed line represents the value of  $F_{\text{BSS/BHB}}$  found in nearby dwarf galaxies by Momany et al. (2007). Corrections for the sampling biases of these populations are described in the text.

proaches increase for larger distances. For this reason, we compared the “as observed” frequency  $F_{\text{BSS/BHB}}$  for both  $R_{\text{D11}}$  and  $R_{\text{FS13}}$ , to gauge the possible impact of choosing one or the other of these calibrations. Results are shown in Figure 9 (values can be found in Table 1). Both frequencies agree within  $3\sigma$ , and the residual values have an average of zero, with a standard deviation of 0.16 kpc. Thus, we choose to employ the calibration from Deason et al. (2011) to represent the distances to BHB stars in the Galactic field, since we found that the introduction of the  $[\text{Fe}/\text{H}]$  as a parameter does not have any impact on the derived distances.

For completeness, Figure 10 shows the derived distances of the BSSs and BHB stars in our sample plotted in the XYZ planes of the Galaxy. As expected, the BHB stars explore to greater distances than the BSSs (and are undersampled in the Solar Neighborhood relative to the BSSs, due to the SDSS bright limit), so care must be taken to account for these limitations in obtaining our final derived relative frequency estimates.

#### 4.3.2. Refined Relative Frequency Estimates

The frequencies presented in Figure 9 were derived to compare the differences resulting from the adoption of different absolute magnitude calibrations. However, as foreshadowed above, we cannot evaluate the value of  $F_{\text{BSS/BHB}}$  in the field without taking into account that there exist regions of the sampled volume that are not simultaneously occupied by BSSs and BHB stars. Near the bright magnitude limit of the SDSS scans ( $g \sim 14.5$ ) the closest selected A-type stars will preferably be BSSs, as BHB stars at similar distances will generally be saturated. Indeed, at  $|Z| < 1$  kpc, our sample includes more than 250 BSSs and only 4 BHB stars. To be safe, we have obtained our counts avoiding the region within  $|Z| = 3$  kpc. At larger distances ( $|Z| > 30$  kpc and  $R > 30$  kpc), our sample preferentially includes BHB stars,

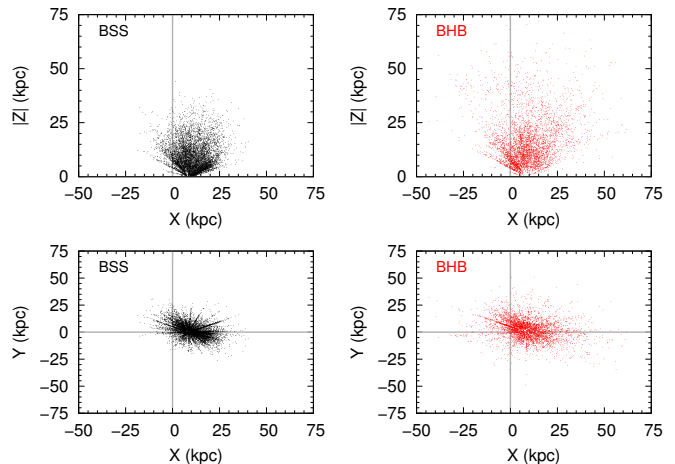


FIG. 10.— Distribution of our sample stars (left panels: BSSs; right panels: BHB stars) in the XZ plane (upper panels), and in the XY plane (the Galactic plane; lower panels). The gray lines are drawn for reference to include the location of the Galactic center.

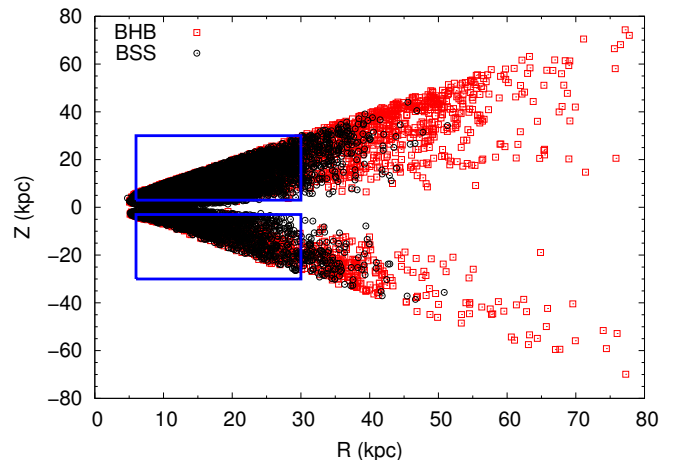


FIG. 11.— Distribution of height above the Galactic plane,  $Z$ , as a function of Galactocentric distance,  $R$ , for the BSSs (black circles) and BHB stars (red squares) in our sample. The blue rectangles limit the regions where we have obtained the relative stellar counts, avoiding the difficulties (under/over counts of BSSs and BHB stars at the bright/faint limits of our sample), as noted in the text:  $3 \text{ kpc} < |Z| < 30 \text{ kpc}$  and  $6 \text{ kpc} < R < 30 \text{ kpc}$ .

and only a few BSSs. Figure 11 summarizes the restrictions we have adopted to derive the relative frequencies,  $F_{\text{BSS/BHB}}$ , shown in Figure 12.

From inspection of Figure 12, the relative blue-straggler frequency in the Galactic halo system is consistent with the value of  $F_{\text{BSS/BHB}}$  obtained for the nearby dwarf galaxies, but not with that obtained for the Solar Neighborhood. The average value of  $F_{\text{BSS/BHB}}$  from  $R = 7$  kpc to  $R = 27$  kpc is  $1.83 \pm 0.23$ .

Preston et al. (1994) evaluated the  $F_{\text{BSS/BHB}}$  in the Solar Neighborhood using stars within 2 kpc of the Sun, a region our data precludes us from exploring. However, we can also examine the  $F_{\text{BSS/BHB}}$  values from another perspective, evaluating the change in frequency with distance from the Galactic plane,  $|Z|$ , from  $|Z| = 3$  kpc to  $|Z| = 30$  kpc, still considering  $R$  between 6 and 30 kpc, as



TABLE 1  
 STELLAR COUNTS IN GALACTOCENTRIC DISTANCE INTERVALS

R(kpc)	Deason et al. (2011)				Fermiani & Schönrich (2013)		
	N <sub>BSS</sub>	N <sub>BHB</sub>	F <sub>BSS/BHB</sub>	$\sigma_{F_{BSS/BHB}}$	N <sub>BHB</sub>	F <sub>BSS/BHB</sub>	$\sigma_{F_{BSS/BHB}}$
06–07	155	99	1.57	±0.14	93	1.67	±0.14
07–08	242	123	1.97	±0.19	129	1.88	±0.21
08–09	293	159	1.84	±0.25	147	1.99	±0.24
09–10	366	140	2.61	±0.23	143	2.56	±0.26
10–11	426	146	2.92	±0.36	130	3.28	±0.35
11–12	501	159	3.15	±0.42	164	3.05	±0.49
12–13	508	208	2.44	±0.46	181	2.81	±0.44
13–14	470	168	2.80	±0.33	181	2.60	±0.40
14–15	483	184	2.63	±0.39	191	2.53	±0.36
15–16	463	220	2.10	±0.36	179	2.59	±0.35
16–17	437	195	2.24	±0.27	202	2.16	±0.36
17–18	465	205	2.27	±0.30	206	2.26	±0.28
18–19	354	201	1.76	±0.30	195	1.82	±0.30
19–20	386	172	2.24	±0.22	180	2.14	±0.23
20–21	318	199	1.60	±0.30	171	1.86	±0.28
21–22	335	147	2.28	±0.20	166	2.02	±0.23
22–23	271	167	1.62	±0.30	162	1.67	±0.26
23–24	207	145	1.43	±0.20	150	1.38	±0.21
24–25	194	135	1.44	±0.17	144	1.35	±0.17
25–26	192	115	1.67	±0.17	127	1.51	±0.16
26–27	140	115	1.22	±0.21	98	1.43	±0.18
27–29	229	173	1.32	±0.15	166	1.38	±0.17
29–32	225	174	1.29	±0.16	216	1.04	±0.17
32–36	166	235	0.71	±0.16	215	0.77	±0.13
36–45	89	407	0.22	±0.09	413	0.22	±0.10
Total	7915	4391	1.80	±0.22	4349	1.82	±0.23

NOTE. — There are 76 BSSs and  $\sim 65$  BHB stars within  $R < 6$  kpc. There are also 10 BSSs and  $\sim 360$  BHB stars that lie between  $45 \text{ kpc} < R < 100 \text{ kpc}$ .

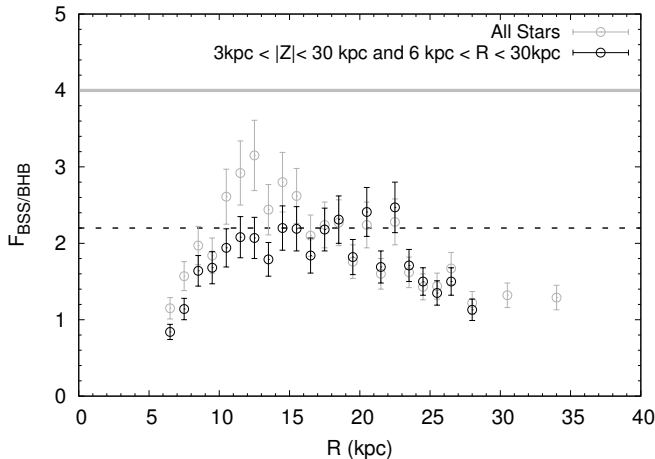


FIG. 12.— Comparison of the relative frequency,  $F_{BSS/BHB}$ , as a function of the Galactocentric distance, for all sample (gray circles) and considering the limited regions defined in Figure 11 (black circles). The gray line represents the value of  $F_{BSS/BHB}$  estimated in the Solar Neighborhood by Preston et al. (1994) and the dashed line represents the value of  $F_{BSS/BHB}$  found in nearby dwarf galaxies by Momany et al. (2007). The  $F_{BSS/BHB}$  found for the Galactic halo system are more consistent with the value of  $F_{BSS/BHB}$  for nearby dwarf galaxies than to that found for the Solar Neighborhood.

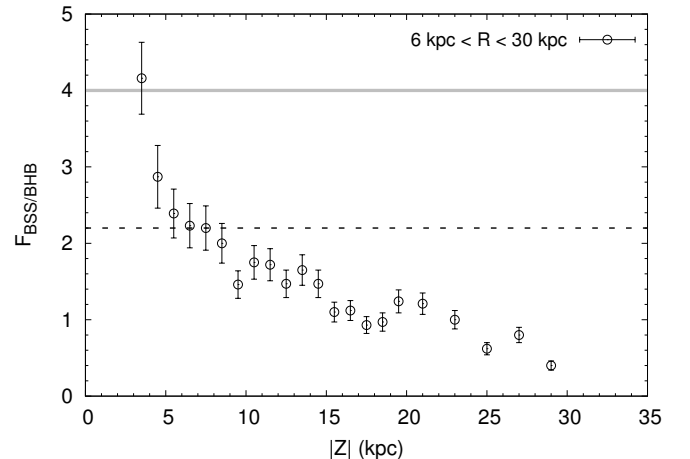


FIG. 13.— Comparison of  $F_{BSS/BHB}$ , as a function of the distance from the Galactic plane,  $|Z|$ , considering the limited regions defined in Figure 11. The gray line represents the value of  $F_{BSS/BHB}$  estimated in the Solar Neighborhood by Preston et al. (1994) and the dashed line represents the value of  $F_{BSS/BHB}$  found in nearby dwarf galaxies by Momany et al. (2007). The relative frequency of BSSs rises closer to the Galactic plane, in agreement with the Solar Neighborhood frequency obtained by Preston et al. (1994).

shown in Figure 13. From inspection of this Figure, the relative frequency of BSSs increases at distances closer to the Galactic plane, reaching a maximum  $F_{BSS/BHB} = 4.11 \pm 0.47$  at  $3 \text{ kpc} < |Z| < 4 \text{ kpc}$ , in agreement with the previous calculation of the Solar Neighborhood frequency.

## 5. POSSIBLE IMPACT OF THE PRESENCE OF STREAMS

It has been shown by a number of recent investigations (e.g., Majewski et al. 2003; Belokurov et al. 2006; Koposov et al. 2012) that the relative importance of debris streams increases with distance from the Galactic center, hence we wish to explore the possible impact of this on our results, making use of our observed stellar

radial velocities.

### 5.1. Distribution of Galactocentric Radial Velocities

Due to their relatively low spatial density, BSSs having  $R > 25$  kpc cannot be readily distinguished as members of stellar streams in the outer region of the Galactic halo based on their distances alone. Analysis of their radial velocities can, however, be used to check for the possible presence of “extragalactic” blue stragglers (i.e., those captured from dissolved satellites) among the stars in the field population.

In order to carry out this analysis, the heliocentric radial velocities ( $V_{\text{HRV}}$ ) of BSSs were converted to the Galactic standard of rest (GSR) frame. The adopted velocity for the Local Standard of Rest ( $V_{\text{LSR}}$ ) is  $220 \text{ km s}^{-1}$ , and a solar motion  $(U, V, W) = (+10.1, +4.0, +6.7) \text{ km s}^{-1}$ , defined in a right-handed Galactic system with  $U$  pointing towards the Galactic center,  $V$  in the direction of Galactic rotation, and  $W$  towards the north Galactic pole (Hogg et al. 2005). Hereafter,  $V_{\text{GSR}}$  is the radial velocity in the GSR frame (i.e., the radial velocity component along the star-Sun direction, corrected for Galactic rotation). Then,

$$V_{\text{GSR}} = V_{\text{HRV}} + (V_{\text{LSR}} + 5.2) \sin l \cos b + 10 \cos l \cos b + 7.2 \sin b. \quad (11)$$

Using the  $V_{\text{GSR}}$  values, one can search for stellar streams associated with the various structural components of the Galaxy, including the thick disk, the inner halo, and the outer halo. By consideration of the different distributions, segregated by distance from the Galactic plane,  $|Z|$ , the inner-halo component of the Milky Way is expected to dominate the population of halo stars found at distances up to  $|Z| \sim 10\text{--}15$  kpc. The outer-halo component is expected to dominate in regions beyond  $|Z| \sim 15\text{--}20$  kpc (Carollo et al. 2007, 2010; Beers et al. 2012). It is important to note that the limits used to separate these in the previous work considered  $Z_{\text{max}}$  and not  $|Z|$ . The derived parameter  $Z_{\text{max}}$  depends on the adopted gravitational potential. In this work we assume that, if there are BSSs whose origin is extragalactic, differences in their radial-velocity distributions in the Galactic standard of rest will be noticed in intervals of either  $Z_{\text{max}}$  or  $|Z|$ .

The velocity distributions of BSSs and BHB stars, considering the approximate limits where each Galactic component becomes dominant, are shown in Figures 14 and 15, respectively. The mean value for the distributions is usually close to zero (with dispersion of about  $100\text{--}150 \text{ km s}^{-1}$ ), representing the typical values of radial velocities for halo stars (Hogg et al. 2005). The mean value of velocities for the BSSs and BHB stars for the most distant stars is shifted toward negative values. This contribution is likely due to a stellar stream, such as Sagittarius, in both the distance from the Galactic center ( $R$  - left panels) and in distance from the Galactic plane ( $|Z|$  - right panels). The dashed lines represent Gaussian fits of these distributions, while the vertical lines indicate their mean values, which are always negative for the most distant stars. These behaviors are evident from inspection of Figures 16 and 17.

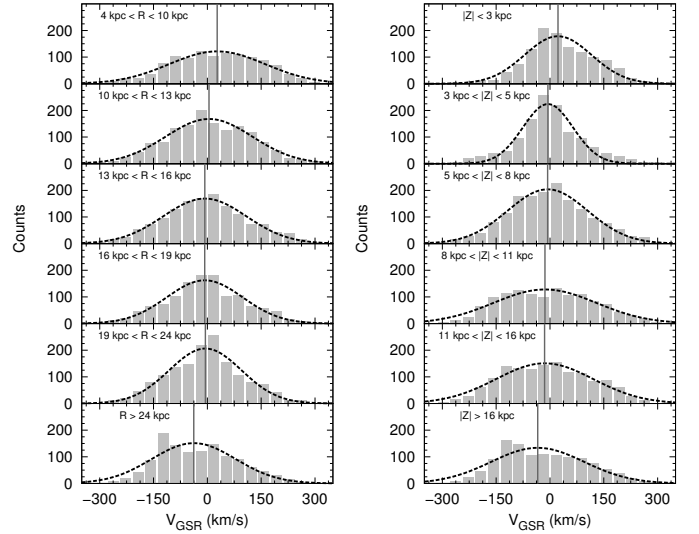


FIG. 14.— Distribution of  $V_{\text{GSR}}$  for BSSs, considering the regions limited by  $R$  (left panels) and  $|Z|$  (right panels). The main distribution found in each panel (usually with mean value close to zero and dispersion of about  $100\text{--}150 \text{ km s}^{-1}$ ) represents typical values of radial velocities for halo stars. The vertical lines show the mean value of  $V_{\text{GSR}}$  for each single Gaussian distribution fitted (dashed black line). It is evident that there is a shift in the mean value of the  $V_{\text{GSR}}$  when we reach the outer-halo region seen in the bottom panels.

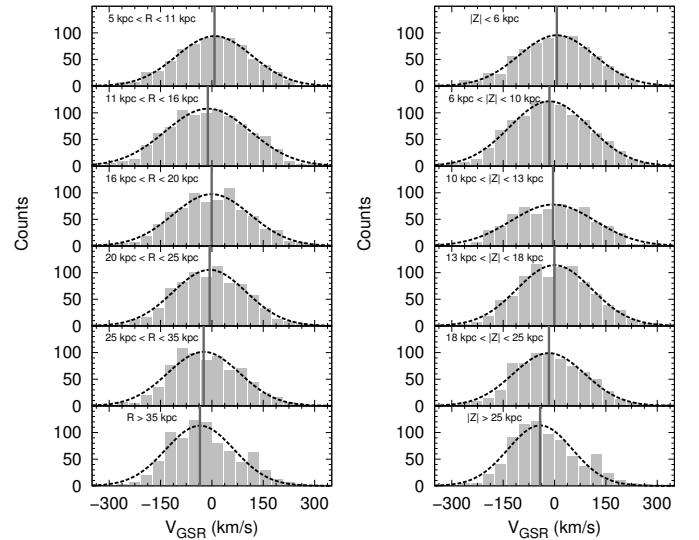


FIG. 15.— Distribution of  $V_{\text{GSR}}$  for BHBs, considering the regions limited by  $R$  (left panels) and  $|Z|$  (right panels). The main distribution found in each panel (usually with mean value close to zero and dispersion of about  $100\text{--}150 \text{ km s}^{-1}$ ) represents typical values of radial velocities for halo stars. The vertical lines show the mean value of  $V_{\text{GSR}}$  for each single Gaussian distribution fitted (dashed black line). It is evident that there is a shift in the mean value of the  $V_{\text{GSR}}$  when we reach the outer-halo region seen in the bottom panels.

### 5.2. Comparison with the Sagittarius Stream

We now compare the  $V_{\text{GSR}}$  for BSSs and BHB stars found at  $|Z| > 17$  kpc with typical values for the Sagittarius Stream (Majewski et al. 2003), in order to verify the hypothesis that at least a portion of the BSSs and BHB stars in our sample can be associated with this stream,

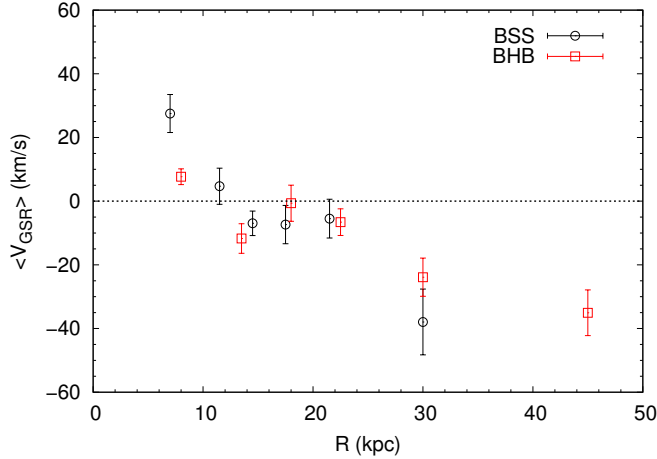


FIG. 16.— Mean values of  $V_{\text{GSR}}$  shown in Figures 14 and 15, as a function of  $R$ . The black circles are the BSSs and the red are the BHBs. Error bars were estimated using the standard deviations of the fitted Gaussians.

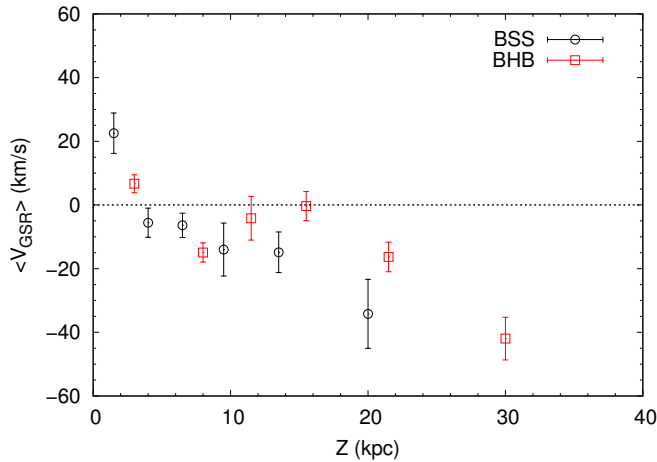


FIG. 17.— Mean values of  $V_{\text{GSR}}$  shown in Figures 14 and 15, as a function of  $|Z|$ . The black circles are the BSSs and the red squares are the BHBs. Error bars were estimated using the standard deviations of the fitted Gaussians.

shown in Figure 18. This Figure highlights the positions (in Galactic coordinates) of BSSs (black circles) and BHB stars (red squares) having velocities in the range  $-200 \text{ km s}^{-1} < V_{\text{GSR}} < -50 \text{ km s}^{-1}$  (the typical Sagittarius Stream range of velocities). From inspection of this Figure, these stars are preferably located over the same coordinates as the Sagittarius Stream (Belokurov et al. 2006; Koposov et al. 2012), highlighted by the large dashed rectangles: (a) In the Northern Galactic Hemisphere, and in (b) the Southern Galactic Hemisphere. The mean heliocentric distance distribution found for both the BSSs and BHBs with these velocities is  $D_{\text{Sg}} = 21.9 \pm 2.2 \text{ kpc}$ . Within  $2\sigma$ , these distances agree with the distance to the Sagittarius Stream measured by Watkins et al. (2009) using RR-Lyræ stars:  $D_{\text{Sg}} = 26.1 \pm 5.6 \text{ kpc}$ . We conclude that at least a portion of the field BSSs and BHB stars are likely to have originated from the Sagittarius Stream, i.e., they are of extragalactic origin.

Figure 19 shows the excess counts of stars relative to

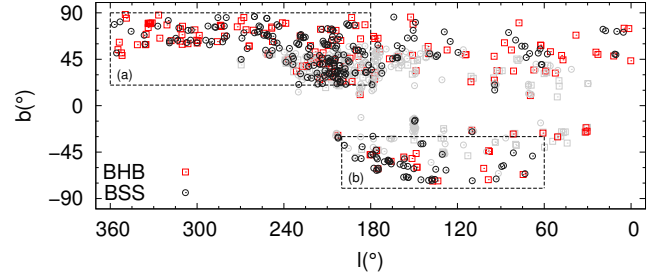


FIG. 18.— Galactic celestial coordinates of BSSs at  $|Z| > 17 \text{ kpc}$  or  $|Z| < 17 \text{ kpc}$  and  $R > 24 \text{ kpc}$ . The BSSs (black circles) and BHB stars (red squares) with  $-200 \text{ km s}^{-1} < V_{\text{GSR}} < -50 \text{ km s}^{-1}$  are preferably located over similar Galactic coordinates as the Sagittarius Stream. The large dashed rectangles highlight the regions where the stream is dominant in (a) The Northern Galactic Hemisphere, and in (b) the Southern Galactic Hemisphere.

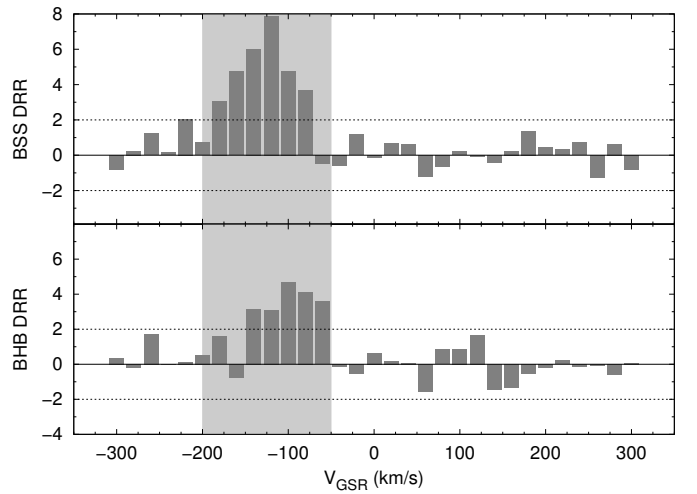


FIG. 19.— Double Residual Root (DRR) plot for the Gaussian fits of the distribution of velocities ( $V_{\text{GSR}}$ ) shown inside the blue rectangles of Figure 11, limited by  $|Z| > 17 \text{ kpc}$ . The top panel shows the BSSs whose velocities suggest association with the Sagittarius Stream (gray shaded region). The bottom panel shows the same distribution for the BHB stars. The dashed lines at  $\pm 2$  indicate an approximate 95% significance level.

the Gaussian fits of the velocity distributions ( $V_{\text{GSR}}$ ) for the BSSs and BHB stars in the blue rectangles of Figure 11, limited by  $|Z| > 17 \text{ kpc}$ . We have employed a variation of a simple difference plot, showing the distribution of the so-called Double Root Residuals (DRRs; see Gebhardt & Beers 1991). The DRR technique takes advantage of the variance-stabilizing properties of a square-root transformation. A DRR plot graphically emphasizes *where* in a distribution there is significant lack of fit between the data and model – the square-root transformation puts the residuals throughout the fit on an equal footing. If the model is an adequate fit to the data, then the DRRs are roughly equivalent to normal deviates. Thus, a DRR with numerical value exceeding  $\pm 2$  is significant at the 95% ( $2\sigma$ ) level, whereas DRRs with absolute magnitude less than 1 indicate a reasonable agreement between data and model.

The top panel of Figure 19 shows the DRRs for BSSs with velocities suggesting association with the Sagittarius Stream (gray shaded region), while the bottom panel

shows the same restrictions for BHB stars. There exists an excess of about  $\sim 400$  BSSs and  $\sim 250$  BHB stars with values of  $V_{\text{GSR}}$  similar to the Sagittarius Stream. This leads to a minimum contamination due to extragalactic BSSs arising from the Sagittarius Stream of about 5% of the total BSS sample. The contamination for BHB stars is even higher, reaching at least 20%. Applying the limits described on Figure 11 and the restrictions of DRR analysis, we found an excess of 246 BSSs and 146 BHB stars in the Sagittarius Stream region. Thus, an estimate of  $F_{\text{BSS/BHB}}$  for the Sagittarius Stream is  $1.68 \pm 0.21$ , in agreement with the mean value of the relative blue-straggler frequency in the Galactic halo and in the nearby dwarf galaxies within  $3\sigma$ . We also verified that the impact of these likely members of the Sagittarius Stream do not change the  $F_{\text{BSS/BHB}}$  values derived by our analysis.

## 6. DISCUSSION AND CONCLUSIONS

We have identified 8001 BSSs and 4796 BHB stars from the SDSS/SEGUE spectroscopic database, obtained through DR8. We find that the BSSs become more frequent than BHB stars for  $g > 17$ , and that the mean value for the blue-straggler frequency in the Galactic halo is  $1.83 \pm 0.23$ , which agrees well with the expected upper limit for BSSs in the nearby dwarf galaxies (Momany et al. 2007,  $\sim 2.2$ ) within  $2\sigma$ . This quantity may be an important input for simulations of stellar populations in the Galaxy, in particular for studies that include BSSs in these calculations (Chen & Han 2009; Conroy & Gunn 2010; Xin et al. 2011; Zhang et al. 2012). We also verified that, for the region closest to the Galactic plane that we can study ( $3 \text{ kpc} < |Z| < 4 \text{ kpc}$ ), the relative frequency of blue stragglers,  $F_{\text{BSS/BHB}} = 4.11$

$\pm 0.47$ , agrees well with Preston et al. (1994) BSSs frequency estimate in the Solar Neighborhood. The relative frequency drops with distance from the plane, reaching  $\sim 1.5 - 2.0$  in the inner-halo region; this ratio continues to decline to  $\sim 1.0$  in the outer-halo region.

Another interesting result from our analysis is the verification of the extragalactic origin of a small fraction ( $\sim 5\%$ ) of BSSs (a somewhat higher fraction,  $\sim 20\%$ , is obtained for BHB stars) found among stars in the outer-halo region.

The distribution of BSSs throughout the Galaxy can be used to constrain how the frequency of primordial binary systems (assuming this is the primary formation channel) varies with distance from the Galactic center. Our analysis indicates that the relative number of BSSs decreases with both  $R$  and  $|Z|$ , thus it would follow that the relative frequency of primordial binary systems should decrease as well.

R.M.S., S.R. and H.M.R. acknowledge CAPES (PROEX), CNPq, PRPG/USP, FAPESP and INCT-A funding. V.M.P. acknowledges support from the Gemini Observatory. T.C.B. acknowledges partial support from grants PHY 08-22648; Physics Frontier Center/JINA, and PHY 14-30152; JINA Center for the Evolution of the Elements (JINA-CEE), awarded by the US National Science Foundation. X.-X. Xue acknowledges the Alexandre Von Humboldt foundation for a fellowship, the DFG's SFB-881 grant "The Milky Way System", and the National Natural Science Foundation of China under grant Nos. 11103031, 11233004, 11390371. The authors would also like to thank the referee, George W. Preston, for his useful comments, and for inspiring this study with his previous work on blue-straggler stars.

## REFERENCES

- Aihara, H., Allende Prieto, C., An, D., Anderson, S. F., Aubourg, É., Balbinot, E., Beers, T. C., Berlind, A. A., Bickerton, S. J., Bizyaev, D., & Blanton, M. R. *et al.* 2011, *ApJS*, 193, 29
- Allende Prieto, C., Sivarani, T., Beers, T. C., Lee, Y. S., Koesterke, L., Shetrone, M., Sneden, C., Lambert, D. L., Wilhelm, R., Rockosi, C. M., Lai, D. K., Yanny, B., Ivans, I. I., Johnson, J. A., Aoki, W., Bailer-Jones, C. A. L., & Re Fiorentin, P. 2008, *AJ*, 136, 2070
- An, D., Johnson, J. A., Clem, J. L., Yanny, B., Rockosi, C. M., Morrison, H. L., Harding, P., & Gunn, J. E. *et al.* 2008, *ApJS*, 179, 326
- Bailyn, C. D. 1995, *ARA&A*, 33, 133
- Beers, T. C., Carollo, D., Ivezić, Ž., An, D., Chiba, M., Norris, J. E., Freeman, K. C., & Lee, Y. S. *et al.* 2012, *ApJ*, 746, 34
- Beers, T. C., Doinidis, S. P., Griffin, K. E., Preston, G. W., & Shectman, S. A. 1992, *AJ*, 103, 267
- Belokurov, V., Zucker, D. B., Evans, N. W., Gilmore, G., Vdrih, S., & Bramich, D. M. *et al.* 2006, *ApJ*, 642, L137
- Boffin, H. M. J., Carraro, G., & Beccari, G. 2014, *ArXiv e-prints*
- Carney, B. W., Latham, D. W., & Laird, J. B. 2005, *AJ*, 129, 466
- Carney, B. W., Latham, D. W., Laird, J. B., Grant, C. E., & Morse, J. A. 2001, *AJ*, 122, 3419
- Carollo, D., Beers, T. C., Chiba, M., Norris, J. E., Freeman, K. C., Lee, Y. S., Ivezić, Ž., Rockosi, C. M., & Yanny, B. 2010, *ApJ*, 712, 692
- Carollo, D., Beers, T. C., Lee, Y. S., Chiba, M., Norris, J. E., Wilhelm, R., Sivarani, T., Marsteller, B., Munn, J. A., Bailer-Jones, C. A. L., Fiorentin, P. R., & York, D. G. 2007, *Nature*, 450, 1020
- Chen, X. & Han, Z. 2009, *MNRAS*, 395, 1822
- Clarkson, W. I., Sahu, K. C., Anderson, J., Rich, R. M., Smith, T. E., Brown, T. M., Bond, H. E., Livio, M., Minniti, D., Renzini, A., & Zoccali, M. 2011, *ApJ*, 735, 37
- Clewley, L., Warren, S. J., Hewett, P. C., Norris, J. E., Peterson, R. C., & Evans, N. W. 2002, *MNRAS*, 337, 87
- Conroy, C. & Gunn, J. E. 2010, *Astrophysics Source Code Library*, 10043
- de Marchi, F., de Angeli, F., Piotto, G., Carraro, G., & Davies, M. B. 2006, *A&A*, 459, 489
- Deason, A. J., Belokurov, V., & Evans, N. W. 2011, *MNRAS*, 416, 2903
- Deason, A. J., Belokurov, V., Evans, N. W., Koposov, S. E., Cooke, R. J., Peñarrubia, J., Laporte, C. F. P., Fellhauer, M., Walker, M. G., & Olszewski, E. W. 2012, *MNRAS*, 425, 2840
- Demarque, P., Woo, J.-H., Kim, Y.-C., & Yi, S. K. 2004, *ApJS*, 155, 667
- Fermani, F. & Schönrich, R. 2013, *MNRAS*, 430, 1294
- Fuhrmann, K. & Bernkopf, J. 1999, *A&A*, 347, 897
- Fusi Pecci, F., Ferraro, F. R., Corsi, C. E., Cacciari, C., & Buonanno, R. 1992, *AJ*, 104, 1831
- Gebhardt, K. & Beers, T. C. 1991, *ApJ*, 383, 72
- Gaspey, J. W., Pritchett, C. J., & Stetson, P. B. 1994, *AJ*, 108, 271
- Hills, J. G. & Day, C. A. 1976, *Astrophys. Lett.*, 17, 87
- Hogg, D. W., Blanton, M. R., Roweis, S. T., & Johnston, K. V. 2005, *ApJ*, 629, 268
- Kinman, T. D., Suntzeff, N. B., & Kraft, R. P. 1994, *AJ*, 108, 1722



- Koposov, S. E., Belokurov, V., Evans, N. W., Gilmore, G., Gieles, M., Irwin, M. J., Lewis, G. F., Niederste-Ostholt, M., Peñarrubia, J., Smith, M. C., Bizyaev, D., Malanushenko, E., Malanushenko, V., Schneider, D. P., & Wyse, R. F. G. 2012, *ApJ*, 750, 80
- Lee, Y. S., Beers, T. C., Allende Prieto, C., Lai, D. K., Rockosi, C. M., Morrison, H. L., Johnson, J. A., An, D., Sivarani, T., & Yanny, B. 2011, *AJ*, 141, 90
- Lee, Y. S., Beers, T. C., Sivarani, T., Allende Prieto, C., Koesterke, L., Wilhelm, R., & Re Fiorentin, P. *et. al.* 2008a, *AJ*, 136, 2022
- Lee, Y. S., Beers, T. C., Sivarani, T., Johnson, J. A., An, D., Wilhelm, R., & Allende Prieto, C. *et. al.* 2008b, *AJ*, 136, 2050
- Leonard, P. J. T. 1989, *AJ*, 98, 217
- Leonard, P. J. T. 1996, in *Astronomical Society of the Pacific Conference Series*, Vol. 90, *The Origins, Evolution, and Destinies of Binary Stars in Clusters*, ed. E. F. Milone & J.-C. Mermilliod, 337
- Majewski, S. R., Skrutskie, M. F., Weinberg, M. D., & Ostheimer, J. C. 2003, *ApJ*, 599, 1082
- Mapelli, M., Sigurdsson, S., Colpi, M., Ferraro, F. R., Possenti, A., Rood, R. T., Sills, A., & Beccari, G. 2004, *ApJ*, 605, L29
- McCrea, W. H. 1964, *Astrophysica Norvegica*, 9, 89
- Momany, Y., Held, E. V., Saviane, I., Zaggia, S., Rizzi, L., & Gullieuszik, M. 2007, *A&A*, 468, 973
- Pier, J. R. 1983, *ApJS*, 53, 791
- Piotto, G., De Angeli, F., King, I. R., Djorgovski, S. G., Bono, G., Cassisi, S., Meylan, G., Recio-Blanco, A., Rich, R. M., & Davies, M. B. 2004, *ApJ*, 604, L109
- Preston, G. W., Beers, T. C., & Shectman, S. A. 1994, *AJ*, 108, 538
- Preston, G. W. & Sneden, C. 2000, *AJ*, 120, 1014
- Preston, G. W. 2014, [arXiv:1406.3468](https://arxiv.org/abs/1406.3468)
- Rocha-Pinto, H. J., Maciel, W. J., & Castilho, B. V. 2001, in *Astronomical Society of the Pacific Conference Series*, Vol. 245, *Astrophysical Ages and Times Scales*, ed. T. von Hippel, C. Simpson, & N. Manset, 364
- Ryan, S. G., Beers, T. C., Kajino, T., & Rosolankova, K. 2001, *ApJ*, 547, 231
- Ryan, S. G., Gregory, S. G., Kolb, U., Beers, T. C., & Kajino, T. 2002, *ApJ*, 571, 501
- Sandage, A. R. 1953, *AJ*, 58, 61
- Sarajedini, A. 1993, in *Astronomical Society of the Pacific Conference Series*, Vol. 53, *Blue Stragglers*, ed. R. A. Saffer, 14
- Sarajedini, A. 1994, *PASP*, 106, 205
- Schlegel, D. J., Finkbeiner, D. P., & Davis, M. 1998, *ApJ*, 500, 525
- Sersic, J. L. 1968, *Atlas de galaxias australes*
- Sirko, E., Goodman, J., Knapp, G. R., Brinkmann, J., Ivezić, Ž., Knerr, E. J., Schlegel, D., Schneider, D. P., & York, D. G. 2004, *AJ*, 127, 899
- Smolinski, J. P., Lee, Y. S., Beers, T. C., An, D., Bickerton, S. J., Johnson, J. A., Loomis, C. P., Rockosi, C. M., Sivarani, T., & Yanny, B. 2011, *AJ*, 141, 89
- Stryker, L. L. 1993, *PASP*, 105, 1081
- Watkins, L. L., Evans, N. W., Belokurov, V., Smith, M. C., Hewett, P. C., Bramich, D. M., Gilmore, G. F., Irwin, M. J., Vidrih, S., Wyrzykowski, L., & Zucker, D. B. 2009, *MNRAS*, 398, 1757
- Wilhelm, R., Beers, T. C., Sommer-Larsen, J., Pier, J. R., Layden, A. C., Flynn, C., Rossi, S., & Christensen, P. R. 1999, *AJ*, 117, 2329
- Xin, Y., Deng, L., de Grijs, R., & Kroupa, P. 2011, *MNRAS*, 411, 761
- Xue, X.-X., Rix, H.-W., Yanny, B., Beers, T. C., Bell, E. F., Zhao, G., Bullock, J. S., Johnston, K. V., Morrison, H., Rockosi, C., Koposov, S. E., Kang, X., Liu, C., Luo, A., Lee, Y. S., & Weaver, B. A. 2011, *ApJ*, 738, 79
- Xue, X. X., Rix, H. W., Zhao, G., Re Fiorentin, P., Naab, T., Steinmetz, M., van den Bosch, F. C., Beers, T. C., Lee, Y. S., & Bell, E. F. *et. al.* 2008, *ApJ*, 684, 1143
- York, D. G., Adelman, J., Anderson, Jr., J. E., Anderson, S. F., Annis, J., Bahcall, N. A., Bakken, J. A., Barkhouser, R., Bastian, S., & Berman, E. *et. al.* 2000, *AJ*, 120, 1579
- Zhang, Y., Han, Z., Liu, J., Zhang, F., & Kang, X. 2012, *MNRAS*, 421, 1678
- Zhao, C. & Newberg, H. J. 2006, [ArXiv: astro-ph/0612034](https://arxiv.org/abs/astro-ph/0612034)